**Supporting Information**

# Integrating metalloporphycenes into p-type NiO-based dye-sensitized solar cells

**Sebastian Feihl,[a] Rubén D. Costa,[a] Wolfgang Brenner,[b] Johannes T. Margraf, [a,c] Rubén Casillas,[a] Oliver Langmar,[a] Anne Browa,[a] Tatyana E. Shubina,[c] Timothy Clark,[c] Norbert Jux,[b] and Dirk M. Guldi[a]**

*[a]Friedrich-Alexander-University Erlangen-Nuremberg, Department of Chemistry and Pharmacy & Interdisciplinary Center for Molecular Materials, Egerlandstr. 3, 91058 Erlangen, Germany. E-mail: dirk.guldi@fau.de, ruben.costa@fau.de. [b]Friedrich-Alexander-University Erlangen-Nuremberg, Department of Chemistry and Pharmacy, Henkestr. 42, 91054 Erlangen, Germany. [c]Friedrich-Alexander-University Erlangen-Nuremberg, Department of Chemistry and Pharmacy, Computer Chemistry Center, Nägelsbachstr. 25, 91052 Erlangen, Germany.*

Synthesis of porphycene sensitizers

Chemicals were purchased from SIGMA-ALDRICH, ACROS ORGANICS, FLUKA, FISHER SCIENTIFIC or ALFA AESAR and used without further purification. All solvents were distilled prior to use. Dichloromethane, chloroform and ethyl acetate were freshly distilled from potassium carbonate. For reactions tetrahydrofuran, dimethylformamide, toluene, and methylene chloride were obtained from VWR as HPLC grade solvents.

Thin Layer Chromatography (TLC) was carried out on aluminum sheets coated with TLC silica gel 60 $F_{254}$ purchased from MERCK. Visualization was performed by using a UV lamp (254 or 366 nm). Flash Column Chromatography (FC) was carried out on silica gel 60 M (deactivated, 230-400 mesh, 0.04-0.063 mm) purchased from MACHEREY-NAGEL or on aluminum oxide (type 507 C neutral, activity I, 100-125 mesh, pH 7.0±0.5; type 5016 A basic, activity I, pH 9.5±0.3) from FLUKA. Eluents were purified as stated above. NMR spectroscopy was conducted using JEOL JNM EX 400, JEOL JNM GX 400, BRUKER Avance 300 and BRUKER Avance 400 machines. All NMR solvents were purchased from EURISO-TOP or DEUTERO. The chemical shifts are reported in parts per million (ppm) and referenced to the residual solvent. Spectral splitting patterns are designated as “s” (singlet), “d” (doublet),

"t" (triplet), "q" (quartet), "m" (multiplet) or as combinations thereof. Signals referred to as "br" (broad) are not clearly resolved or significantly broadened. The raw data was processed using MestReNova LITE and ACD Labs 12.0. If a chemical shift is stated twice, the two corresponding signals are clearly separated from each other, but the peak positions are rounded to the same value. The atom numbers of the protons responsible for the stated signal are in *italics*. When one and the same signal is caused by two or more protons, the atom numbers are connected by "/". With signals that originate from multiple protons and their resonances coinciding in one multiplet, the assigned groups are stated separately. A number in brackets indicates how many groups contribute to the signal, respectively. IR spectroscopy was performed on a BRUKER FT-IR Tensor 27 and Pike MIRacle ATR unit. The ATR unit was equipped with a diamond crystal plate and high-pressure clamp. Spectra were recorded as solid samples directly from the diamond crystal with the probe on top. All absorptions $\nu$ are given in wave-numbers [$cm^{-1}$]. UV/Vis spectroscopy was carried out on a VARIAN Cary 5000 UV-Vis-NIR Spectrometer. Spectra were recorded at room temperature using quartz cuvettes with a path length of 1 cm in the indicated solvents. The baseline was corrected before the measurements were taken. The absorption maxima $\lambda_{max}$ are given in [nm] with the extinction coefficients in [$M^{-1}cm^{-1}$]. Mass spectrometry (MS) was done on a SHIMADZU AXIMA Confidence MALDI-TOF MS-Spectrometer (nitrogen UV-laser, 50 Hz, 337 nm) with 2,5-dihydroxybenzoic acid (DHB), trans-2-(3-(4-*t*-butylphenyl)-2-methyl-2-propenylidene)-malononitrile (DCTB) or sinapic acid (sin) used as matrices. EI mass spectra were recorded on a FINNIGAN MAT 95 XP. ESI mass spectrometry was carried out on a BRUKER maXis 4G UHR TOF MS/MS-Spectrometer or a BRUKER micrOTOF II focus TOF MS-Spectrometer. 2,7,12,17-tetra-*n*-propylporphycenato nickel(II) **1** were synthesized according to the literature. [1, 2]

**3-Formylvinyl-2,7,12,17-tetra-*n*-propylporphycenato nickel(II) 2 and**

**9-Formylvinyl-2,7,12,17-tetra-*n*-propylporphycenato nickel(II) 3**

Phosphoryl chloride (1.17 ml, 12.7 mmol) was slowly added to 3-dimethylaminoacrolein (1.26 ml, 12.6 mmol) dissolved in 21 ml dry methylene chloride. After stirring for six hours a solution of 2,7,12,17-tetra-*n*-propylporphycenato nickel(II) **2** (210 mg, 0.392 mmol) in 80 ml dry methylene chloride was added slowly and then the reaction mixture was stirred overnight. 70 ml of a saturated sodium bicarbonate solution were added and the mixture was heated at reflux for 30 minutes. The solution was allowed to cool to room temperature and the layers were separated. The organic layer was washed with water twice, stripped of solvent and purified by column chromatography (silica gel, eluent: chloroform / hexanes = 3 / 1). The green 9-formylvinyl-2,7,12,17-tetra-*n*-propylporphycenato nickel(II) **3** was eluted first followed by the blue 3-formylvinyl-2,7,12,17-tetra-*n*-propylporphycenato nickel(II) **2**.

**3-Formylvinyl-2,7,12,17-tetra-*n*-propyl-porphycenato nickel(II) 2**

Yield: 35.5 mg (60.2 μmol, 15.4%)

$^{1}$H NMR (400 MHz, rt, $CDCl_3$): δ = 9.89 (d, 1H, $^{3}J$ = 7.6 Hz, C*H*O), 9.10 (d, 1H, $^{3}J$ = 11.2 Hz, pyrrole-C*H*CH-pyrrole), 9.06 (d, 1H, $^{3}J$ = 11.2 Hz, pyrrole-CHC*H*-pyrrole), 9.02 (d, 1H, $^{3}J$ = 11.2 Hz, pyrrole-C*H*CH-pyrrole), 8.84 (d, 1H, $^{3}J$ = 11.2 Hz, pyrrole-CHC*H*-pyrrole), 8.70 (m, 2H, *13*/*16*), 8.25 (d, 1H, $^{3}J$ = 16.0 Hz, porphycene-C*H*CH), 8.19 (s, 1H, *6*), 6.78 (dd, 1H, $^{3}J$ = 16.0 Hz, $^{3}J$ = 7.6 Hz, porphycene-CHC*H*), 3.79 (m, 4H, C$H_2$$CH_2CH_3$), 3.59 (t, 2H, $^{3}J$ = 7.8 Hz, C$H_2$$CH_2CH_3$), 3.27 (t, 2H, $^{3}J$ = 8.0 Hz, C$H_2$$CH_2CH_3$), 2.29 (m, 4H, $CH_2$C$H_2$$CH_3$), 2.10 (tq, 2H, $^{3}J$ = 7.5 Hz, $^{3}J$ = 7.5 Hz, $CH_2$C$H_2$$CH_3$), 1.90 (tq, 2H, $^{3}J$ = 7.5 Hz, $^{3}J$ = 7.5 Hz, $CH_2$C$H_2$$CH_3$), 1.34 (t, 3H, $^{3}J$ = 7.3 Hz, $CH_2CH_2$C$H_3$), 1.34 (t, 3H, $^{3}J$ = 7.3 Hz, $CH_2CH_2$C$H_3$), 1.25 (t, 3H, $^{3}J$ = 7.3 Hz, $CH_2CH_2$C$H_3$), 1.18 (t, 3H, $^{3}J$ = 7.3 Hz, $CH_2CH_2$C$H_3$) ppm.

$^{13}$C NMR (100.5 MHz, rt, $CDCl_3$): δ = 194.2, 150.5, 150.0, 149.7, 147.9, 146.8, 146.5, 145.4, 144.3, 143.8, 143.5, 142.7, 142.1, 140.6, 130.9, 126.0, 119.7, 119.6, 118.7, 108.5, 108.4, 107.1, 107.0, 31.0, 31.0, 29.3, 26.3, 25.1, 24.7, 24.7, 14.7, 14.5, 14.5 ppm.

MS (MALDI-TOF, without matrix): m/z = 588 $[M]^+$.

HRMS (ESI) for $C_{35}H_{38}N_4NiO$: calc.: 588.239361

found: 588.239165

UV/Vis ($CH_2Cl_2$): $\lambda_{max}$ (ε [$M^{-1}cm^{-1}$]) = 265 (23000), 306 (20900), 396 (79300), 624 (49000) nm.

IR (ATR, rt): $\nu$ = 667, 720, 741, 763, 788, 805, 827, 885, 923, 941, 966, 983, 1034, 1060, 1104, 1121, 1145, 1234, 1249, 1283, 1307, 1319, 1454, 1464, 1495, 1518, 1561, 1597, 1619, 1656, 1669, 2866, 2928, 2956 $cm^{-1}$.

**9-Formylvinyl-2,7,12,17-tetra-*n*-propyl-porphycenato nickel(II) 3**

Yield: 54.1 mg (91.8 µmol, 23.4%)

$^1$H NMR (400 MHz, rt, $CDCl_3$): δ = 9.54 (d, 1H, $^3J$ = 7.8 Hz, C*H*O), 9.18 (d, 1H, $^3J$ = 11.2 Hz, pyrrole-C*H*CH-pyrrole), 9.12 (d, 1H, $^3J$ = 11.2 Hz, pyrrole-CHC*H*-pyrrole), 8.57 (s, 1H, porphycene-*H*), 8.44 (s, 1H, porphycene-H), 8.34 (s, 2H, porphycene-*H*), 8.07 (s, 1H, porphycene-*H*), 7.92 (d, 1H, $^3J$ = 15.4 Hz, porphycene-C*H*CH), 6.47 (dd, 1H, $^3J$ = 15.4 Hz, $^3J$ = 7.8 Hz, porphycene-CHC*H*), 3.77 (m, 4H, C$H_2$CH$_2$CH$_3$), 3.77 (t, 2H, $^3J$ = 7.8 Hz, C$H_2$CH$_2$CH$_3$), 2.71 (t, 2H, $^3J$ = 7.8 Hz, C$H_2$CH$_2$CH$_3$), 2.28 (m, 4H, CH$_2$C$H_2$CH$_3$), 2.09 (m, 2H, CH$_2$C$H_2$CH$_3$), 1.74 (m, 2H, CH$_2$C$H_2$CH$_3$), 1.34 (t, 3H, $^3J$ = 7.3 Hz, CH$_2$CH$_2$C$H_3$), 1.33 (t, 3H, $^3J$ = 7.3 Hz, CH$_2$CH$_2$C$H_3$), 1.22 (t, 3H, $^3J$ = 7.3 Hz, CH$_2$CH$_2$C$H_3$), 1.02 (t, 3H, $^3J$ = 7.3 Hz, CH$_2$CH$_2$C$H_3$) ppm.

$^{13}$C NMR (100.5 MHz, rt, $CDCl_3$): δ = 193.3, 160.6, 150.9, 150.3, 146.7, 144.0, 143.5, 143.3, 142.1, 141.5, 127.8, 121.3, 119.0, 118.5, 115.9, 108.4, 107.6, 107.1, 35.6, 31.0, 30.9, 30.6, 29.7, 24.8, 24.7, 24.1, 23.8, 22.6, 14.6, 14.6, 14.4, 14.3 ppm.

MS (MALDI-TOF, without matrix): m/z = 588 $[M]^+$.

HRMS (ESI) for $C_{35}H_{39}N_4NiO$: calc.: 589.247186
found: 589.245707

UV/Vis ($CH_2Cl_2$): $\lambda_{max}$ (ε [$M^{-1}cm^{-1}$]) = 267 (29800), 284 (25700), 305 (24100), 417 (84500), 624 (64900) nm.

IR (ATR, rt): $\nu$ = 681, 745, 804, 834, 890, 909, 930, 943, 977, 1009, 1043, 1072, 1106, 1130, 1230, 1247, 1283, 1299, 1462, 1571, 1602, 1665, 2868, 2924, 2955 $cm^{-1}$.

**$3^4$-Dicarboxy-buta-$3^1$,$3^3$-dienyl-2,7,12,17-tetra-*n*-propyl-porphycenato nickel(II) P1**

3-Formylvinyl-2,7,12,17-tetra-*n*-propyl-porphycenato nickel(II) **2** (13.6 mg, 23.1 µmol), malonic acid (24.0 mg, 230 µmol) and ammonium acetate (18.0 mg, 230 µmol) were dissolved in 6 ml of a mixture of tetrahydrofuran and acetic acid (1/1). The reaction mixture was heated at 70 °C for 90 minutes and allowed to cool down to room temperature. After the addition of water it was filtrated. The residue was taken up in tetrahydrofuran, stripped of solvent with a stream of $N_2$ gas and purified by column chromatography (silica gel, eluent:

methylene chloride / methanol / acetic acid = 900 / 115 / 13.5). The solvent was removed with a stream of $N_2$ gas and porphycene **P1** was obtained as a dark green powder.

Yield: 8.8 mg (13.0 µmol, 56.4%)

$^1$H NMR and $^{13}$C NMR: As already reported in the literature for similar molecules the strong aggregation does not allow an interpretation of the spectra. [3]

MS (MALDI-TOF, DHB): m/z = 674 $[M]^+$.

HRMS (ESI) for $C_{38}H_{39}N_4NiO_4$: calc.: 673.233027

found: 673.233577

IR (ATR, rt): $\nu$ = 617, 675, 693, 744, 760, 807, 889, 927, 973, 982, 1036, 1056, 1104, 1172, 1240, 1281, 1319, 1375, 1453, 1490, 1509, 1561, 1703, 2869, 2929, 2957 $cm^{-1}$.

**$9^4$-Dicarboxy-buta-$9^1$,$9^3$-dienyl-2,7,12,17-tetra-*n*-propyl-porphycenato nickel(II) P2**

9-Formylvinyl-2,7,12,17-tetra-*n*-propyl-porphycenato nickel(II) **3** (20 mg, 33.9 µmol), malonic acid (35 mg, 340 µmol) and ammonium acetate (26 mg, 340 µmol) were dissolved in 6 ml of a mixture of tetrahydrofuran and acetic acid (1/1). The reaction mixture was heated at 70 °C for one hour and allowed to cool down to room temperature. After the addition of water it was filtrated. The residue was taken up in tetrahydrofuran, stripped of solvent with a stream of $N_2$ gas and purified by column chromatography (silica gel, eluent: methylene chloride / methanol / acetic acid = 900 / 115 / 13.5). The solvent was removed with a stream of $N_2$ gas to yield porphycene **P2** as a dark green powder.

Yield: 10.5 mg (15.5 µmol, 45.9%)

$^1$H NMR and $^{13}$C NMR: As already reported in the literature for similar molecules the strong aggregation does not allow an interpretation of the spectra.[3]

MS (MALDI-TOF, DHB): m/z = 674 $[M]^+$.

HRMS (ESI) for $C_{38}H_{39}N_4NiO_4$: calc.: 673.23303

found: 673.23238

IR (ATR, rt): $\nu$ = 618, 660, 741, 804, 907, 976, 1026, 1047, 1106, 1175, 1247, 1303, 1375, 1397, 1458, 1544, 1561, 2870, 2929, 2957 $cm^{-1}$.

**$9^4$-Carboxy-$9^4$-cyano-buta-$9^1$,$9^3$-dienyl-2,7,12,17-tetra-*n*-propyl-porphycenato nickel(II) P3**

9-Formylvinyl-2,7,12,17-tetra-*n*-propyl-porphycenato nickel(II) **3** (20 mg, 33.9 µmol), cyanoacetic acid (29 mg, 340 µmol) and ammonium acetate (26 mg, 230 µmol) were dissolved in 6 ml of a mixture of tetrahydrofuran and acetic acid (1/1). The reaction mixture

was heated at 70 °C for one hour and allowed to cool down to room temperature. After the addition of water it was filtrated. The residue was taken up in tetrahydrofuran, stripped of solvent with a stream of $N_2$ gas and purified by column chromatography (silica gel, eluent: methylene chloride / methanol / acetic acid = 1928.5 / 115 / 13.5). The solvent was removed with a stream of $N_2$ gas and porphycene **P3** was obtained as a dark green powder.

Yield: 16.6 mg (25.3 µmol, 74.6%)

$^1$H NMR (400 MHz, rt, THF-$d_8$): δ = 9.00 (d, 1H, $^3J$ = 11.0 Hz, pyrrole-C*H*CH-pyrrole), 8.93 (d, 1H, $^3J$ = 11.0 Hz, pyrrole-CHC*H*-pyrrole), 8.44 (s, 1H, porphycene-*H*), 8.30 (s, 1H, porphycene-*H*), 8.12 (s, 1H, porphycene-*H*), 7.83 (s, 1H, porphycene-*H*), 7.73 (s, 1H, porphycene-*H*), 7.66 (d, 1H, $^3J$ = 11.5 Hz, C*H*-C(CN)-$CO_2$H), 6.87 (d, 1H, $^3J$ = 14.5 Hz, porphycene-C*H*CH), 6.72 (dd, 1H, $^3J$ = 14.5 Hz, $^3J$ = 11.5 Hz, porphycene-CHC*H*), 3.66 (m, 4H, C*H*$_2$CH$_2$CH$_3$), 3.04 (t, 2H, $^3J$ = 6.8 Hz, C*H*$_2$CH$_2$CH$_3$), 2.24 (m, 6H, C*H*$_2$CH$_2$CH$_3$ / CH$_2$C*H*$_2$CH$_3$(2x) ), 1.94 (m, 2H, CH$_2$C*H*$_2$CH$_3$), 1.52 (m, 2H, CH$_2$C*H*$_2$CH$_3$), 1.35 (m, 6H, CH$_2$CH$_2$C*H*$_3$), 1.20 (t, 3H, $^3J$ = 6.8 Hz, CH$_2$CH$_2$C*H*$_3$), 0.92 (t, 3H, $^3J$ = 6.7 Hz, CH$_2$CH$_2$C*H*$_3$) ppm.

$^{13}$C NMR (100.5 MHz, rt, THF-$d_8$): δ = 164.4, 155.6, 155.4, 151.7, 150.7, 150.6, 147.3, 147.1, 146.6, 145.3, 144.7, 144.5, 143.9, 142.7, 142.3, 123.4, 121.7, 120.2, 119.7, 119.2, 117.6, 115.7, 109.2, 108.4, 107.8, 104.8, 36.1, 31.7, 31.6, 31.4, 24.3, 15.0, 14.9, 14.9, 14.6 ppm.

MS (MALDI-TOF, without matrix): m/z = 655 $[M]^+$.

HRMS (ESI) for $C_{38}H_{38}N_5NiO_2$: calc.: 654.23845
found: 654.23862

IR (ATR, rt): $\nu$ = 657, 686, 801, 847, 906, 931, 975, 1044, 1075, 1109, 1142, 1171, 1244, 1268, 1317, 1377, 1418, 1462, 1566, 1589, 1677, 1714, 2870, 2929, 2958 cm$^{-1}$.

Experimental details

Steady-state UV-Vis absorption spectroscopy of **P1**, **P2**, and **P3** in DMF ($c = 10^{-5}$ M) was recorded with a Shimadzu UV-3102 PC UV-Vis-NIR Scanning Spectrophotometer in the range 300 – 750 nm.

Square wave voltammetry was performed in a range between -1.7 to +1.7 V – Figure S13 and Table S5. The porphycenes **P1**, **P2**, and **P3** were dissolved in DMF. The concentration was kept at $c = 10^{-4}$ M. Tetrabutylammonium hexafluorophosophate (TBAFP) was used as conducting salt (c = 0.1 M). Ferrocene redox couple ($Fc/Fc^{+}$) was used as electrochemical reference. The scan rate was adjusted to 0.05 V $s^{-1}$. The setup consisted of a graphite working electrode, a platinum wire as counter and a silver wire as a quasi reference electrode. All measurements were performed after saturating the solvent with argon for at least 10 mins and keeping the argon flow overlaying the solution during the data recording.

Fabrication of transparent p-type NiO electrodes was performed by preparing a precursor solution. In details, 1 g of $NiCl_2$ (Aldrich, 98 %) and 1 g of Synperonic F108 (Fluka) were dissolved in a flask containing a mixture of 3 ml of Millipore water and 8 ml of ethanol. Stirring led to a clear green solution that was rested for 3 days at 30 °C. Centrifugation (Thermo Scientific Multifuge X1R equipped with Fiberlite F15 rotor) was performed at 12,000 rpm for 3 h in order to remove microcrystals, which prevent the formation of suitable films. Previous to film processing, fluorine doped tin oxide glass slides (FTO, 8 Ω/square, Pilkington, XOP Glass, Spain) were successively cleaned with isopropanol, 0.1 M hydrochloric acid solution, tenside solution, water, and isopropanol by means of ultrasonication (Elma Elmasonic P, frequency at 37 kHz, power at 100 %) for 15 min at each step, followed by cleaning in a ozone lamp (JELIGHT COMPANY, INC. UVO-Cleaner Model # 342-220) for 20 min. NiO films were processed with the help of a rackel machine (Zehnter ZAA 2300) and a Scotch® tape mask on the FTOs. After baking at 400 °C for 30 min in a muffle furnace (Nabertherm L9/11 P330) the resulting electrodes were characterized by means of field-emission scanning electron microscopy (Zeiss Gemini 55 Ultra), X-ray diffraction (Bruker D8 Advance, λ (Cu Kα) = 0.154 nm), steady-state UV-Vis absorption spectroscopy (Jenoptik Specord S600), and profilometry (Bruker Dektak XT). In line with the SEM images (Figure S5), profilometry indicates an electrode thickness of 1.2 µm. The transparency of the NiO electrodes was proven by UV-Vis transmission spectroscopy, showing a high transparency of up to 90 % from 350 to 750 nm – Figure S7.

The XRD spectrum reveals the face centered cubic crystallinity of the NiO - Figure S6. Using the full width at half maximum of the (200) NiO peak and the Debye-Scherrer equation (1), the size of nanoparticles was estimated to be at around 16.4 nm. [4]

$$L = \frac{K \cdot \lambda}{(\beta \cdot cos\theta)} \qquad (1)$$

$L$ as the size of nanoparticles that can also be expressed by $L = p \cdot d_{hkl}$ ($p$ is the Number of the lattice planes, $d_{hkl}$ is the distance between them). The factor $\beta$ is the full width at half maximum (FWHM) in radian, which is measured at the glancing angle $\theta$. Furthermore, $K$ is the form factor, which is defined by the form of the crystallites. If the crystallite is supposed to be spherical, $K$ equals 0.89.

In order to get insight into the dye adsorption behavior on the NiO electrodes steady-state UV-Vis absorption kinetics were performed. Therefore, the transparent NiO electrodes were soaked into the corresponding dye solutions of **P1**, **P2** and **P3** (c = $10^{-4}$ M). The absorption was subsequently monitored for every 10 min during the first 30 min by following the increase of the Q-band of the dyes that were adsorbed on the electrodes. Then the time steps were increased to 30 min until 150 min overall soaking time. The stagnating absorption of the sensitized NiO electrodes that became already apparent after 90 min induces that the maximum of the dye uptake process had finished and that a monolayer of dye molecules was established on the NiO surface. Bathochrome red shifts of the observed Q-bands (**P1**: 620 nm → 632 nm, **P2**: 628 nm → 638 nm, **P3**: 627 nm → 641 nm) indicated successful immobilisation of the porphycenes as shown for **P2** - Figure S9.

The sensitized electrodes were finally assembled with a platinum covered counter electrode in order to test the different porphycenes in relation to their ability to work as sensitizers in p-type dye-sensitized solar cells (DSSCs). Construction of the counter electrode was done by drilling two holes of 1 mm in diameter into a FTO slide and subsequently cleaning of the slide as described above. Finally, the conductive surface of the FTO substrate was covered with a 5 mM solution of $H_2PtCl_6$ (Aldrich, ~ 38 % Pt) by drop-casting and then backed at 390 °C for 15 min. The p-type NiO photocathode and the counter electrode were placed together using a Syrlin foil (Solaronix, 25 µm) while the space between the two electrodes was filled with electrolyte. The latter consisted of a mixture of LiI and $I_2$ (molar ratio of 5 : 1) in acetonitrile. The concentration of LiI was 1.0 M. The prepared p-type NiO DSSCs were measured under standard conditions, that is AM 1.5 and incident light power density $P_0$ = 100 mW·cm$^{-2}$. Photocurrent (J-V) curves were monitored with a potentiostat (Metrohm Autolab AUT 83394, Nova 1.9) in the voltage range -0.2 to +0.05 V. The

measurements were performed for at least 5 devices of each type in order to test the reproducibility of the results.

By using characteristic data points in the J-V curves such as the open-circuit voltage ($V_{oc}$), the short-current density ($J_{sc}$), the current-density and the voltage at the maximum power point ($J_m$ and $V_m$, respectively), the fill factor (2) and the efficiency (3) as important parameters were calculated

$$FF = \frac{J_m \cdot V_m}{J_{sc} \cdot V_{oc}} \qquad (2)$$

$$\eta = \frac{J_{sc} \cdot V_{oc} \cdot FF}{P_0} \qquad (3)$$

Incident-photon-to-current-efficiency (IPCE) was recorded in the range between 350 to 780 nm by illuminating the p-type NiO DSSCs with a xenon arc lamp over a Cornerstone 260 1/4 m Monochromator equipped with a Merlin digital radiometric lock-in-system.

Long term photostability for all porphycenes was proven by periodically measuring the absorption of sensitized transparent NiO electrodes by means of steady-state UV/Vis absorption spectroscopy in the wavelength range where only the absorption features of the dye were present, meaning from 550 to 750 nm. In this range absorption or reflection features of the NiO electrodes did not influence the measurements. The soaking conditions were set in correlation to the results from the absorption kinetics measurements. Starting with a measurement at every 10 min for the first 30 min, the intervals time was set to 30 min until an overall time of 120 min was reached. 16 h after the beginning of the series a last measurement was performed. In order to proof if the evaluation process on the p-DSSC devices has any effect on the stability of the porphycene sensitizers steady-state UV/Vis absorption spectroscopy of the dyed electrodes was additionally measured. Therefore, the electrodes were irradiated under AM 1.5 conditions, and their UV/Vis spectra were continuously recorded every 5 min for the first two minutes, then in 10 min intervals until the time period reached 70 min – Figure S11.

Electrochemical impedance spectroscopy (EIS) was performed under light and dark conditions. Measurements were performed under $V_{oc}$ conditions in a frequency range of 0.01 Hz to 100 kHz. The voltage amplitude was set to be 10 mV. The received impedance data in the form of Nyquist plots was fitted by using the Nova 1.9 software to a circuit model that simulates the impedance of interfaces between the different components of DSSCs – Figure S13. [5] It consists of a sequential arrangement of sheet resistance $R_s$ and two resistances $R_1$

and $R_2$, the latter each in parallel with the corresponding constant phase elements $CPE_1$ and $CPE_2$. $R_s$ represents all the ohmic series resistances of the FTO substrates, and electrical contacts. The $R_1$ and the $CPE_1$ both relate to the electrolyte/platinum counter electrode interface in the high frequency range. Here, the charge transfer from the platinum counter electrode to the electrolyte takes place. In addition, charge recombination processes at NiO electrode/sensitizer/electrolyte interface is linked to $R_2$ and $CPE_2$. The earlier presents the charge transfer resistance either in the light ($R_i$) or in the dark ($R_d$), while the latter is related to the chemical capacitance. [5, 6] Finally, the fitting results of the $CPE_2$ were transformed in pseudo capacitances $C_2$, giving a realistic picture of the electrical properties of at the NiO electrodes. The recombination constant $k_{eff}$ for the back reaction under light conditions was determined by taking the frequency at the maximum $\omega_{max}$ of the arc in the Nyquist plot that was related to $R_2$ (6). [7]

$$k_{eff} = \omega_{max} \qquad (6)$$

Finally, the hole lifetime $\tau_h$ in the NiO electrode was calculated from the Bode phase plots. The frequency of the maximum $f_{max}$ corresponding to the response of the NiO electrode in the low frequency range was used for this purpose (7). [8]

$$\tau_h = \frac{1}{2\pi f_{max}} \qquad (7)$$

The data received from EIS in the dark gives a clear overview about the processes at the electrode/electrolyte interface when the sensitizer is not being excited. [5, 9, 10] Recombination at this interface in absence of the sensitizer can be evaluated by fitting the Nyquist plot in accordance to the circuit model - Figures S14 and S15, Tables S5 and S6.

Computational calculations

Semiempirical UHF and UNO-PECI calculations were performed with VAMP 11.0 using the PM6 Hamiltonian. [11-14] The geometry of the NiO cluster was fixed at the experimental crystal structure of bulk NiO during the simulations.

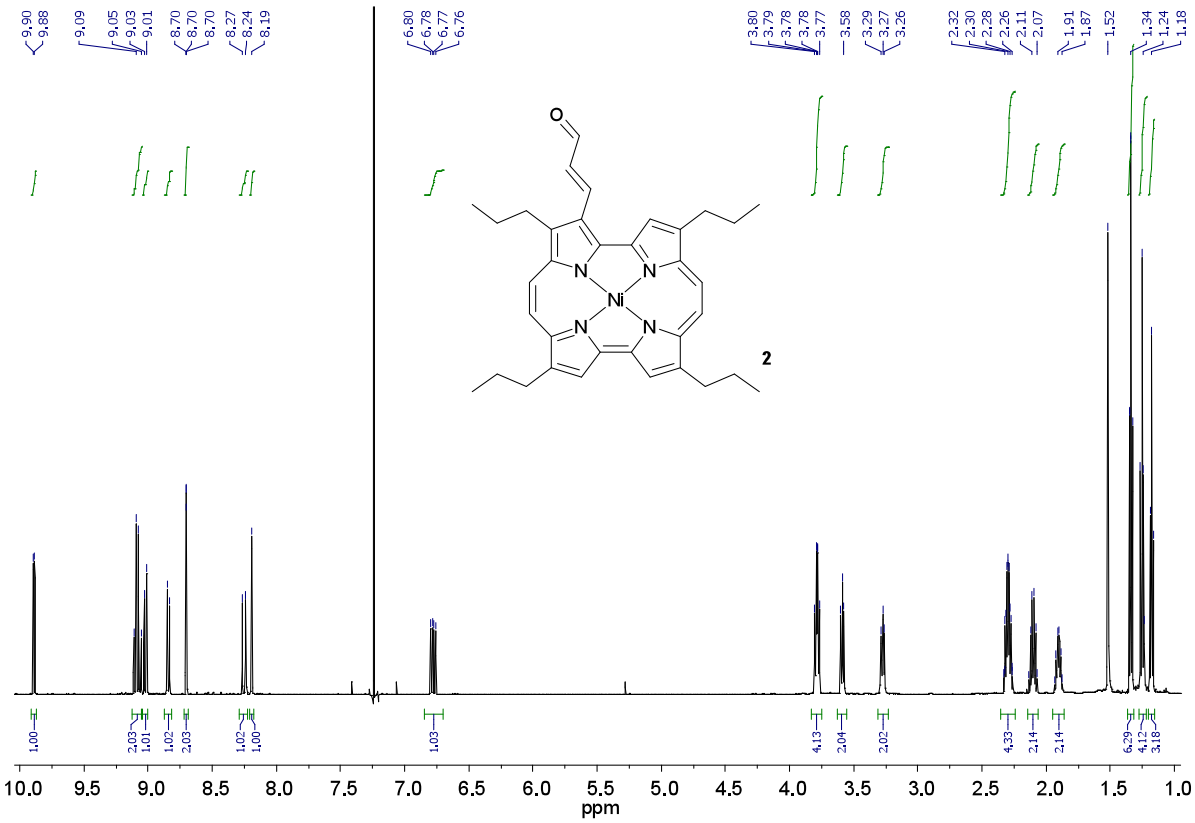


**Figure S1a** $^{1}$H NMR spectrum of **2** (400 MHz, rt, $CDCl_3$)

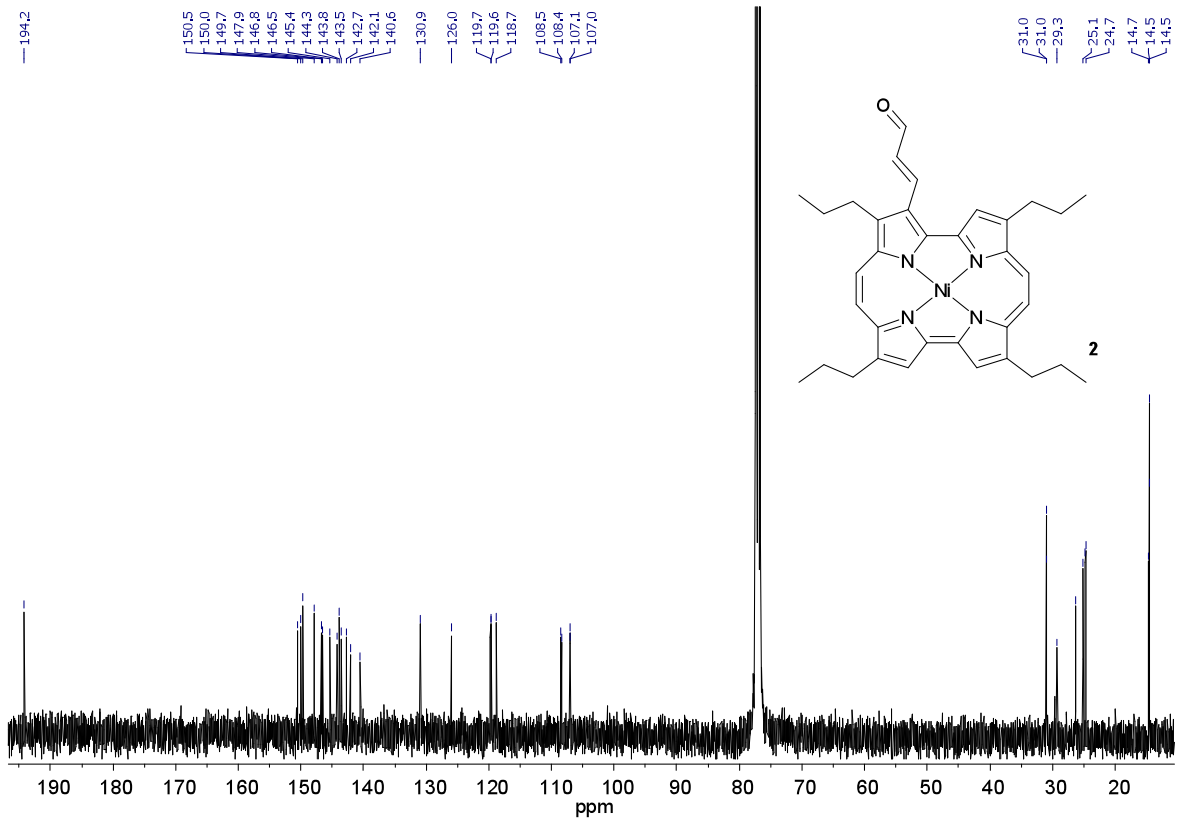


**Figure S1b** $^{13}$C NMR spectrum of **2** (100.5 MHz, rt, $CDCl_3$).

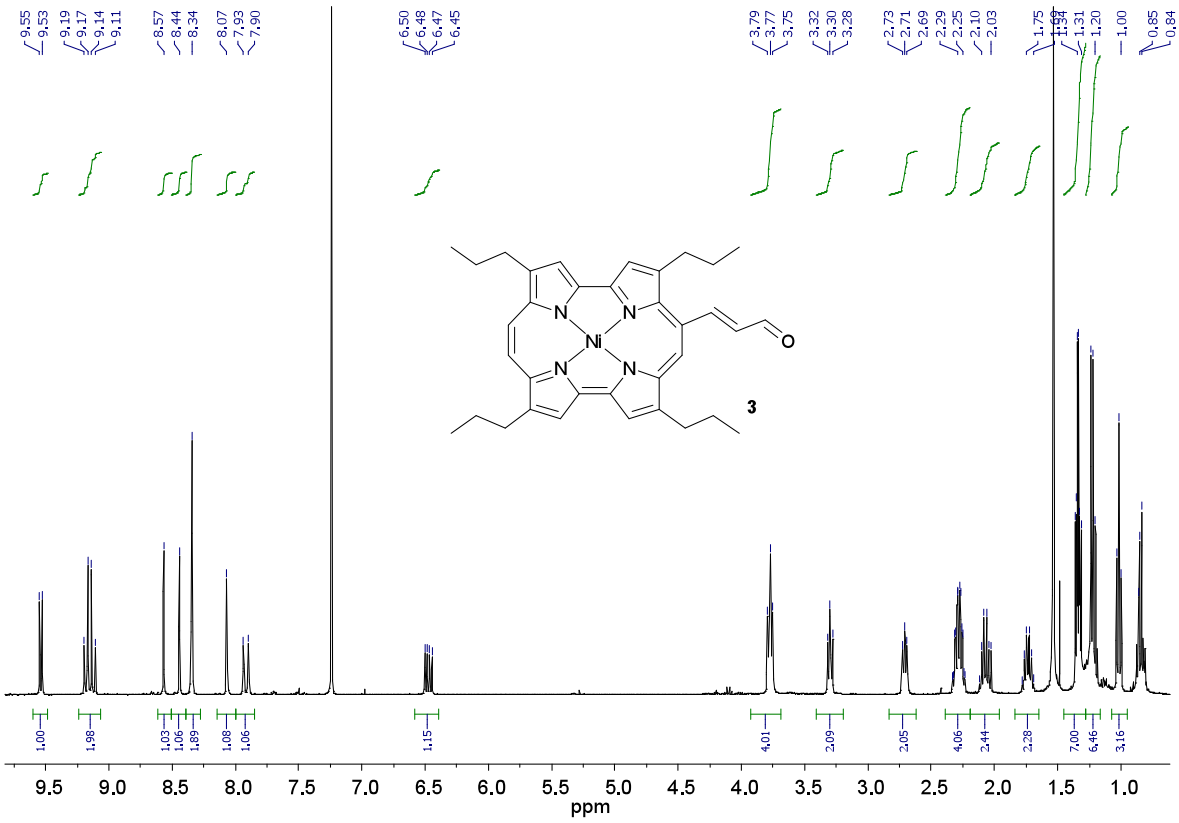


**Figure S2a** $^{1}$H NMR spectrum of **3** (400 MHz, rt, $CDCl_3$).

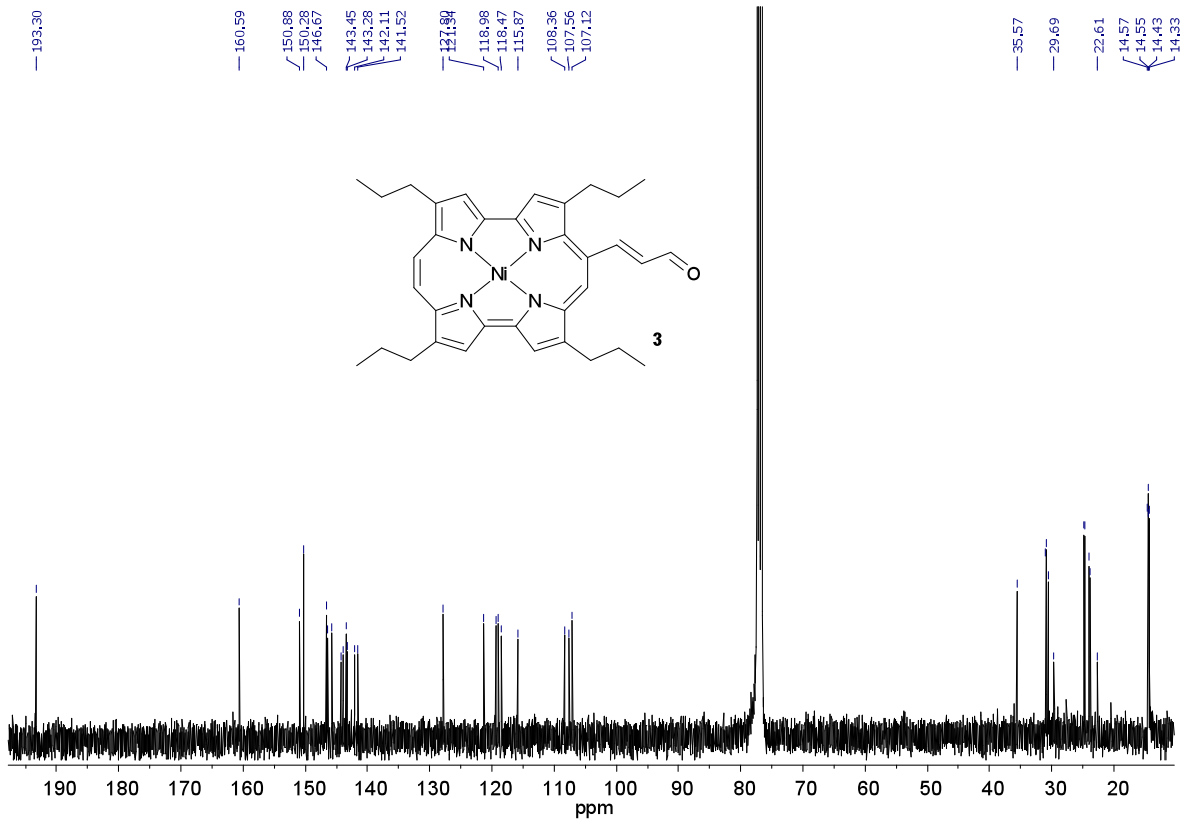


**Figure S2b** $^{13}$C NMR spectrum of **3** (100.5 MHz, rt, $CDCl_3$).

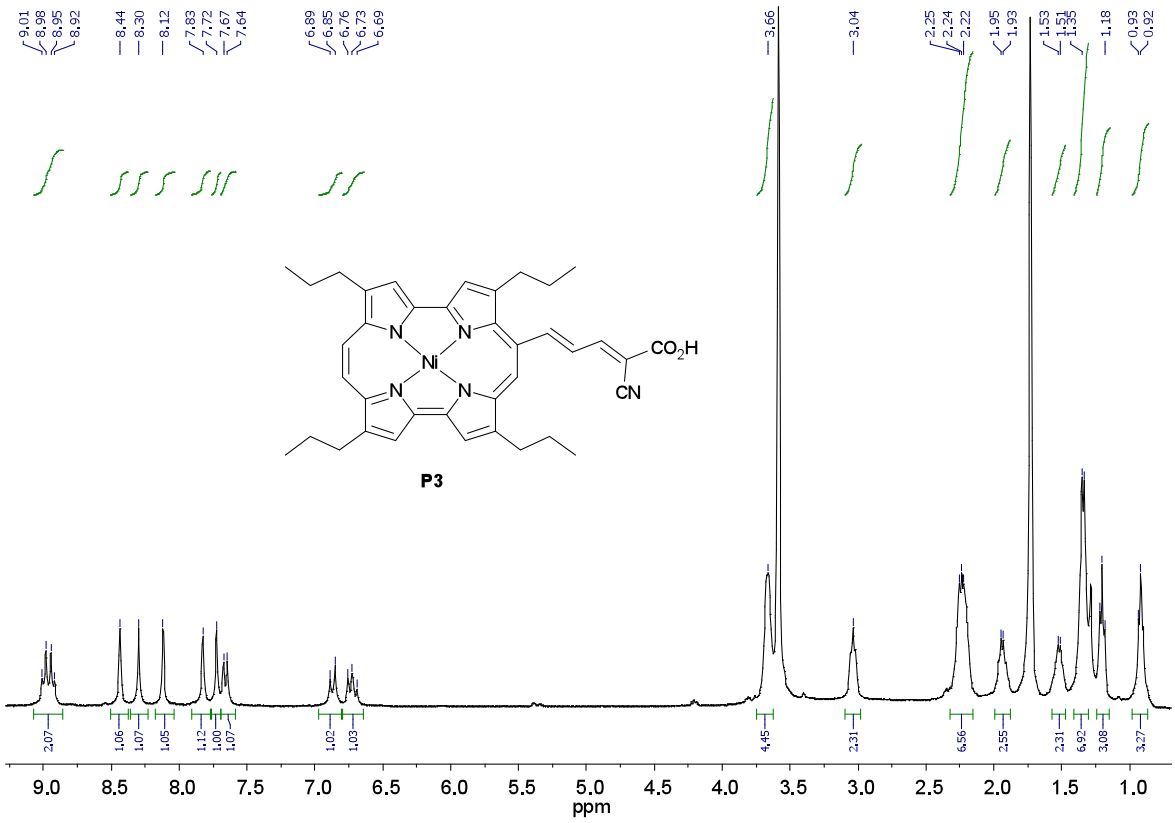


**Figure S3a** $^{1}$H NMR spectrum of **P3** (400 MHz, rt, THF-$d_8$).

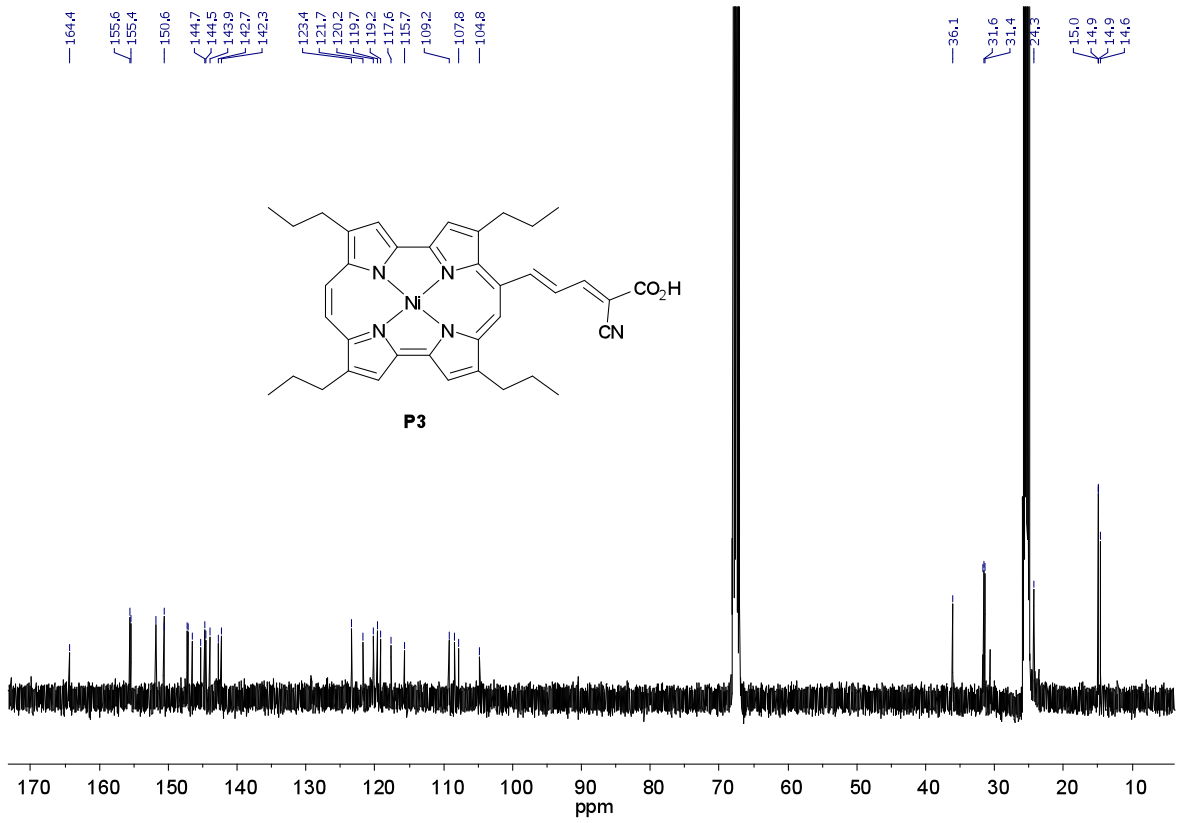


**Figure S3b** $^{13}$C NMR spectrum of **P3** (100.5 MHz, rt, THF-$d_8$).

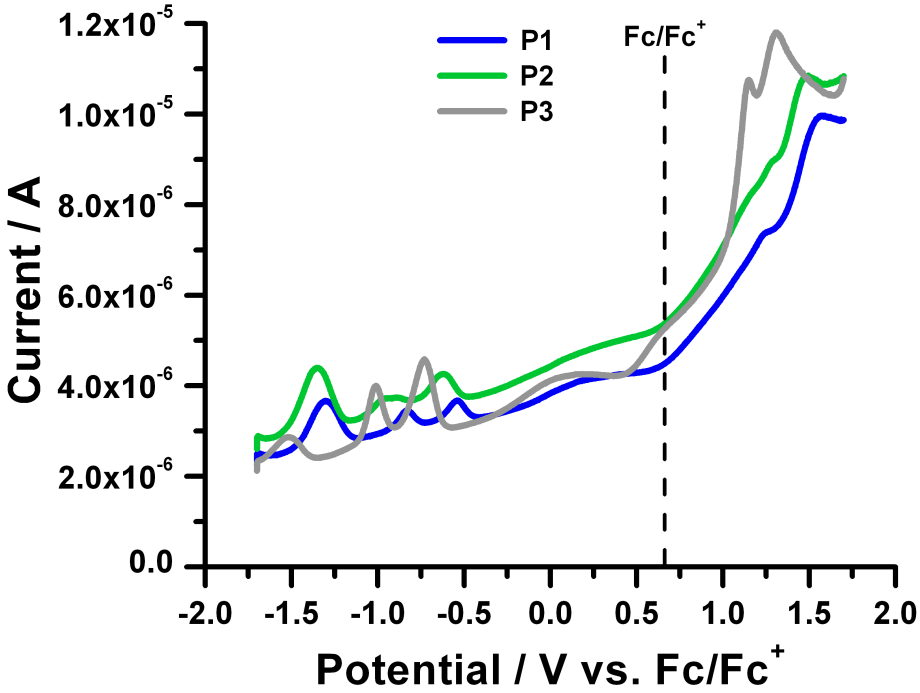


**Figure S4** Square wave voltammograms of **P1**, **P2**, and **P3** ($10^{-4}$ M) in DMF. Tetrabutylammonium hexafluorophosophate (TBAFP) was used as supporting electrolyte (0.1 M). Ferrocene redox couple ($Fc/Fc^{+}$) is represented by dashed line at 0.66 V was used as reference. Scan rate was adjusted to 0.05 $V \cdot s^{-1}$.

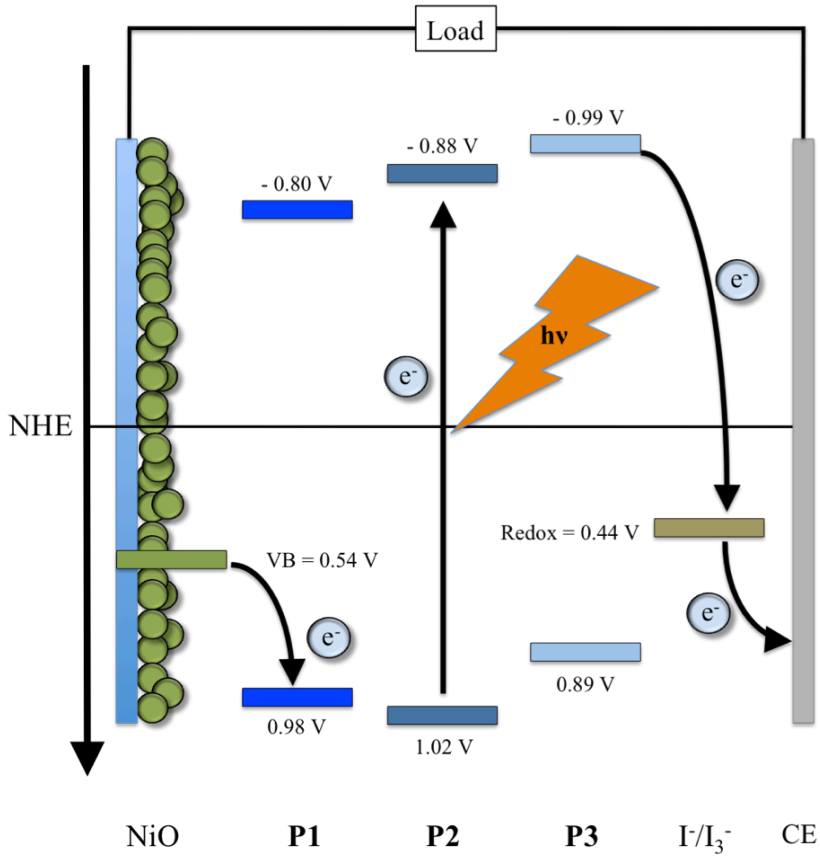


**Figure S5** Reduction and oxidation potentials of **P1**, **P2**, and **P3** in reference to the valence band (VB) of NiO and to the redox potential of the $I_3^-/I^-$ couple. All potentials are given versus normal hydrogen electrode (NHE).

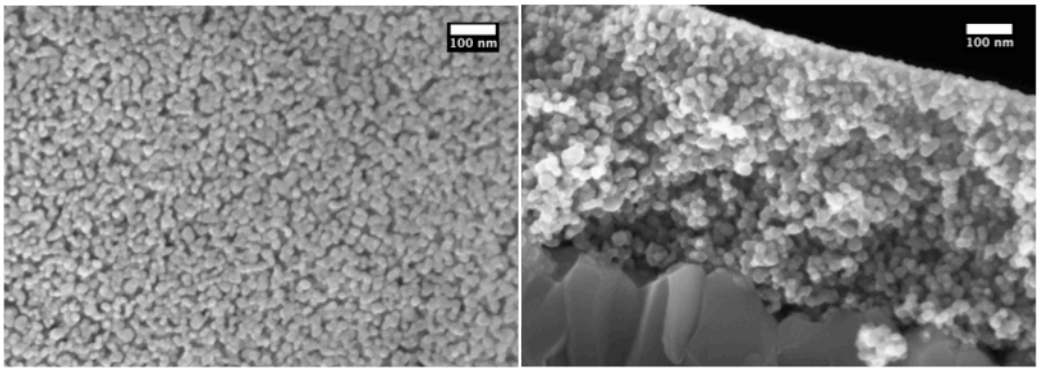


**Figure S6** SEM images of transparent NiO electrodes – top view on the left and cross sectional view on the right.

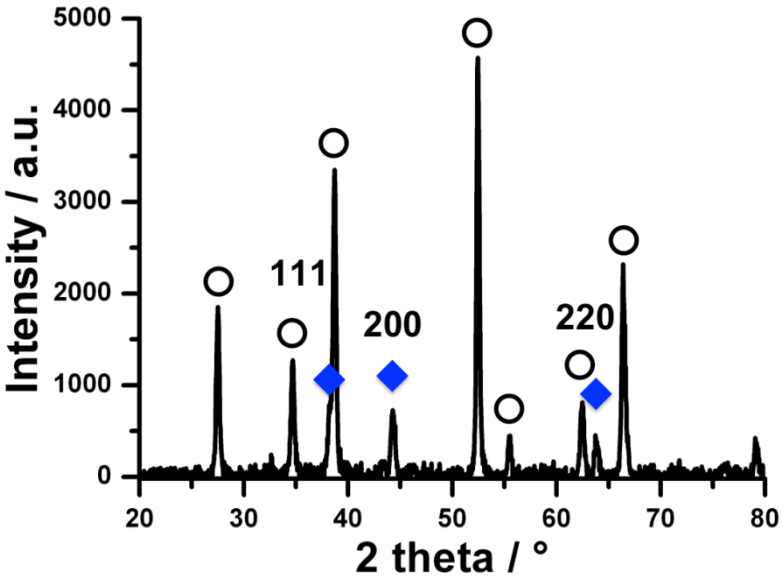


**Figure S7** X-ray diffraction (XRD) pattern of NiO on FTO. The characteristic peaks of face centered cubic NiO are clearly identified (diamonds) despite the presence of the FTO signals (circles).

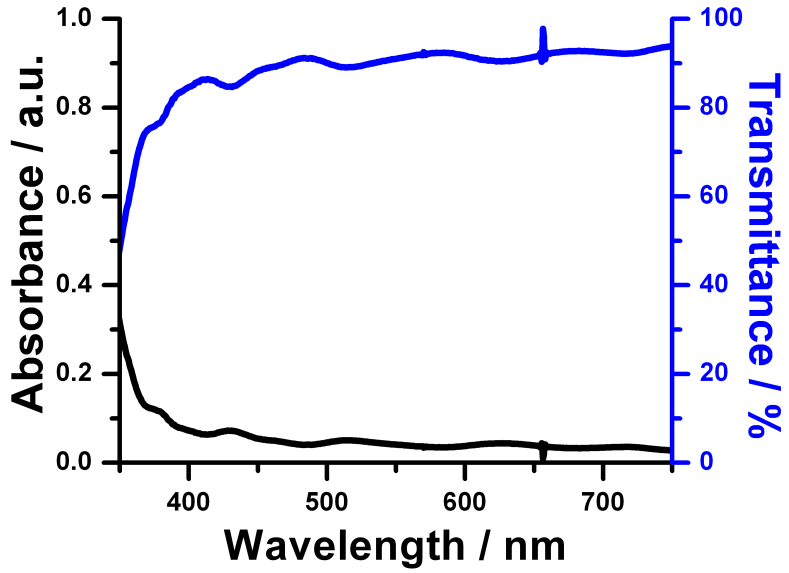


**Figure S8** Steady-state absorption and transmission spectra of the transparent NiO electrode.

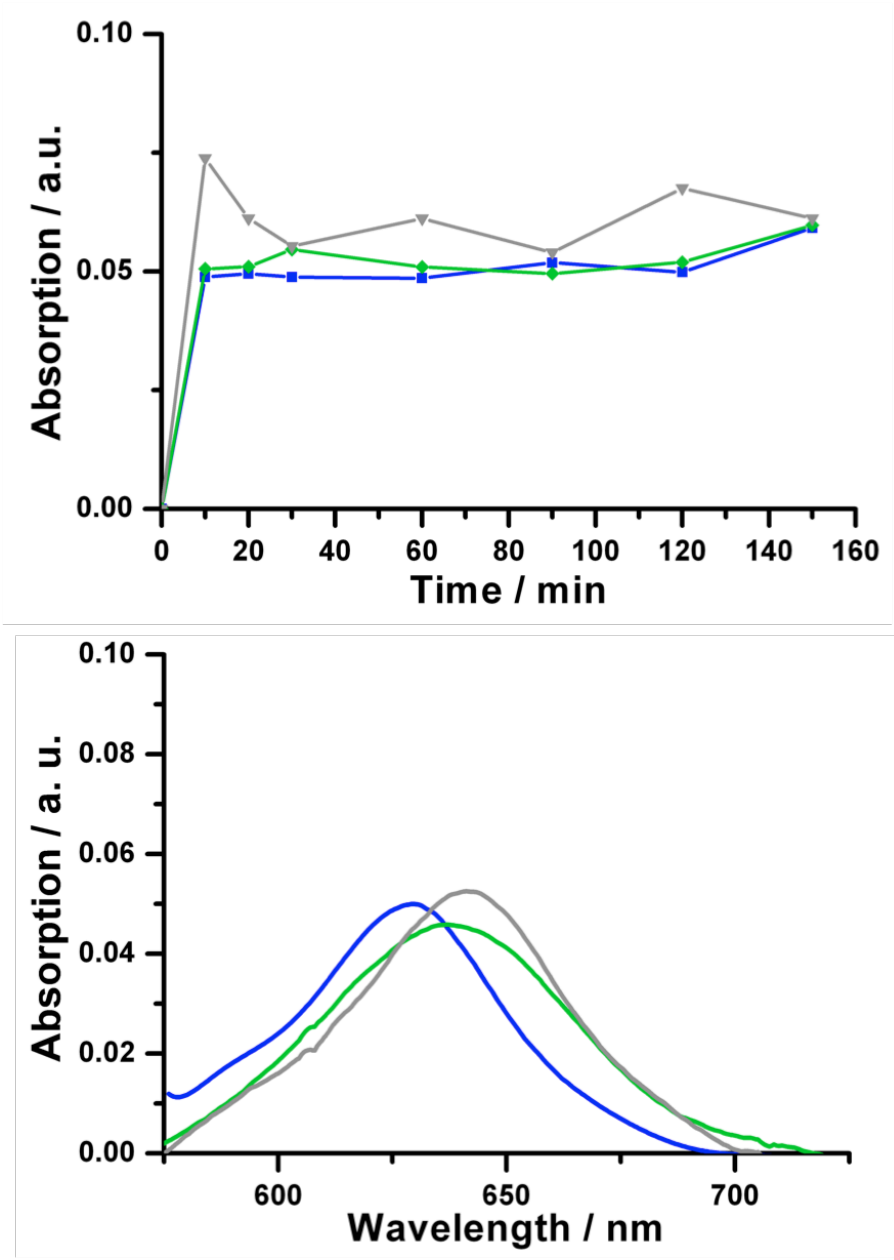


**Figure S9** Upper part – Absorption kinetics of **P1** (blue), **P2** (green) and **P3** (grey) recorded at the maxima of steady-state absorption spectra of the dyed transparent NiO electrodes for increasing soaking times (**P1** at 630 nm, **P2** at 638 nm, and **P3** at 641 nm). The NiO electrodes were soaked in DMF solution, c = $1.0 \cdot 10^{-4}$ M. Lower part – steady-state absorption spectra recorded after 90 min for **P1**, **P2** and **P3** on transparent NiO electrodes.

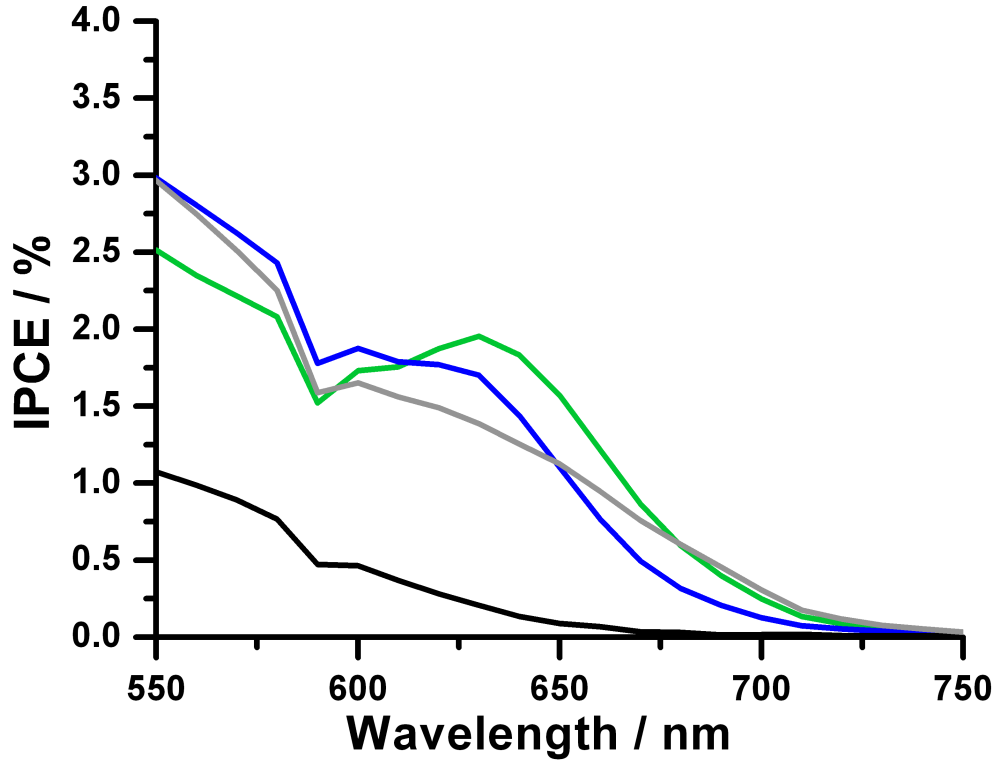


**Figure S10** IPCE spectra of p-type NiO DSSCs sensitized with **P1** (blue), **P2** (green), **P3** (grey) and a bare NiO electrode (black).

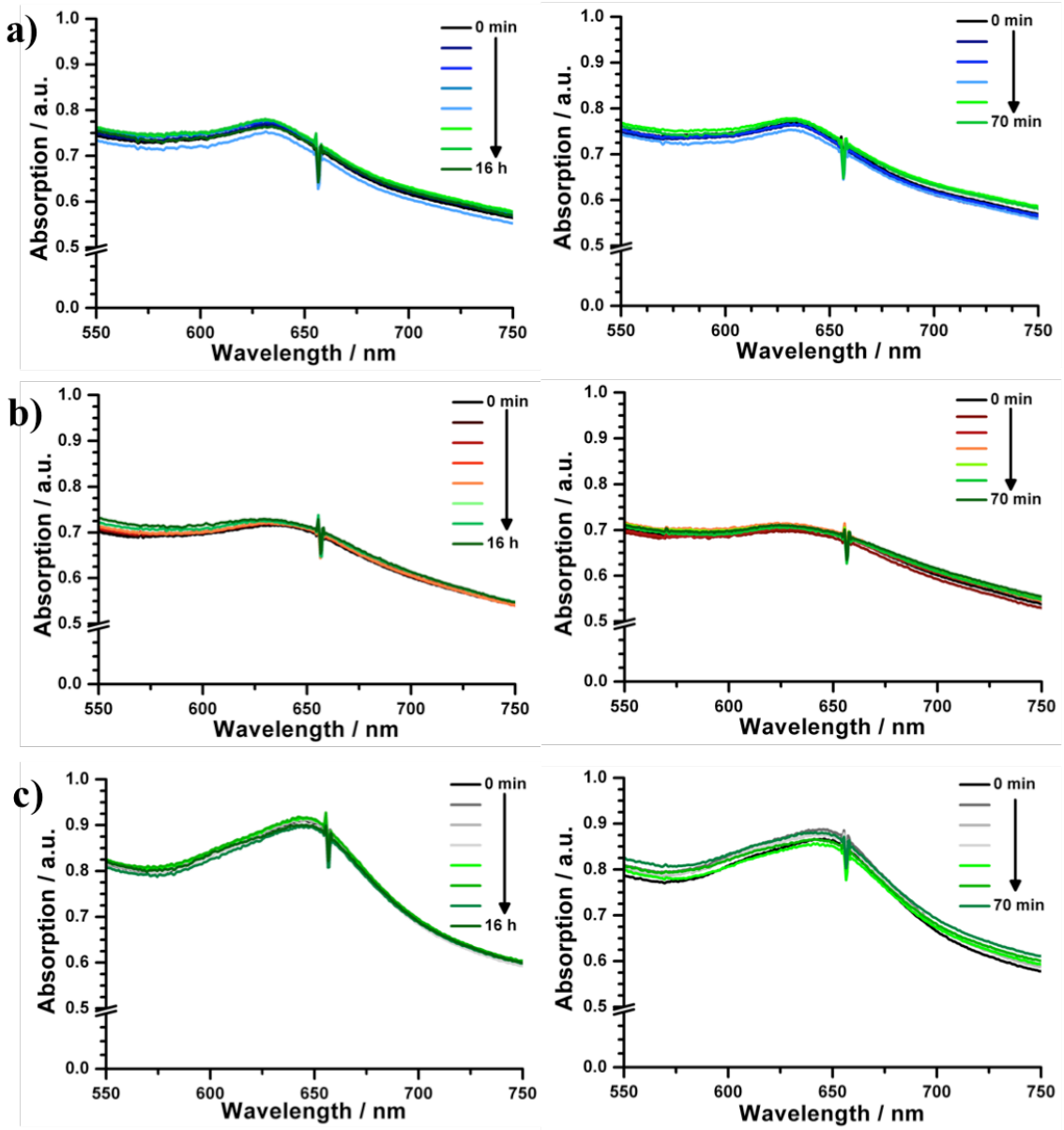


**Figure S11** Absorption spectra of **P1** (a), **P2** (b) and **P3** (c) attached onto transparent NiO electrodes over the time under ambient light (left) and 1 sun/ AM 1.5 illumination (right) conditions.

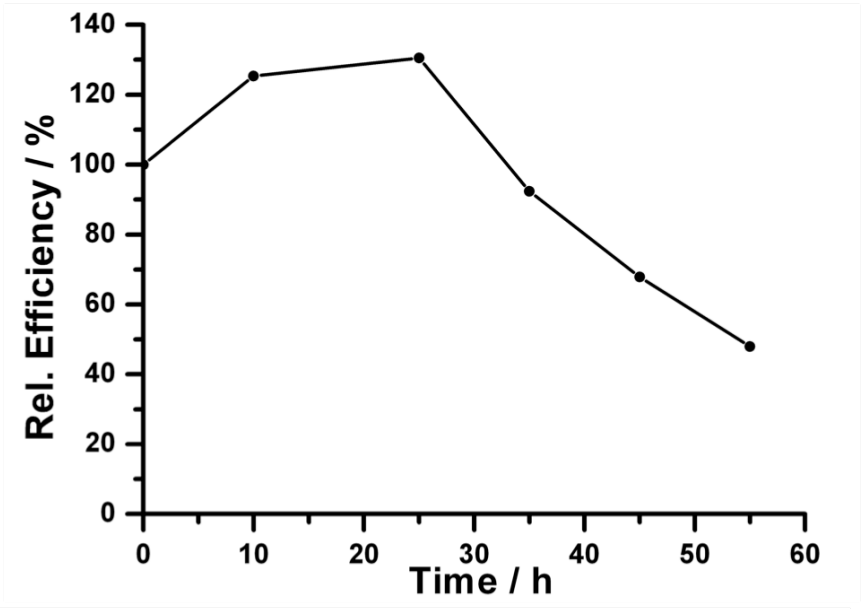


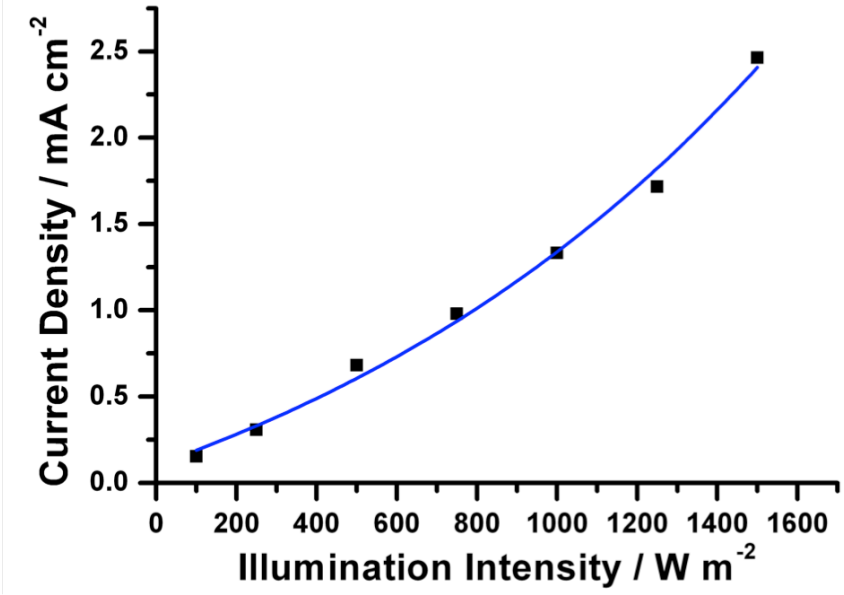


**Figure S12** Upper-part - Relative efficiency versus time plot of **P2** sensitized NiO p-type DSSC. Lower Part – Correlated current density versus illumination intensity plot. The fitting is represented by the blue line.

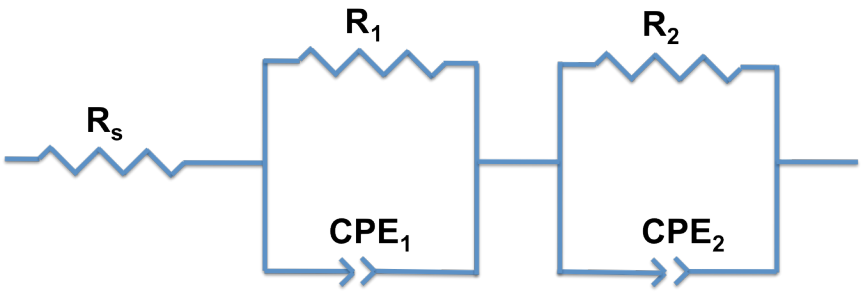


**Figure S13** Circuit model that was used to fit the electrochemical impedance spectroscopy (EIS) data. Here, $R_2$ and $CPE_2$ (constant phase element) represent the resistance and the chemical capacitance at the electrode/sensitizer/electrolyte interface. [5]

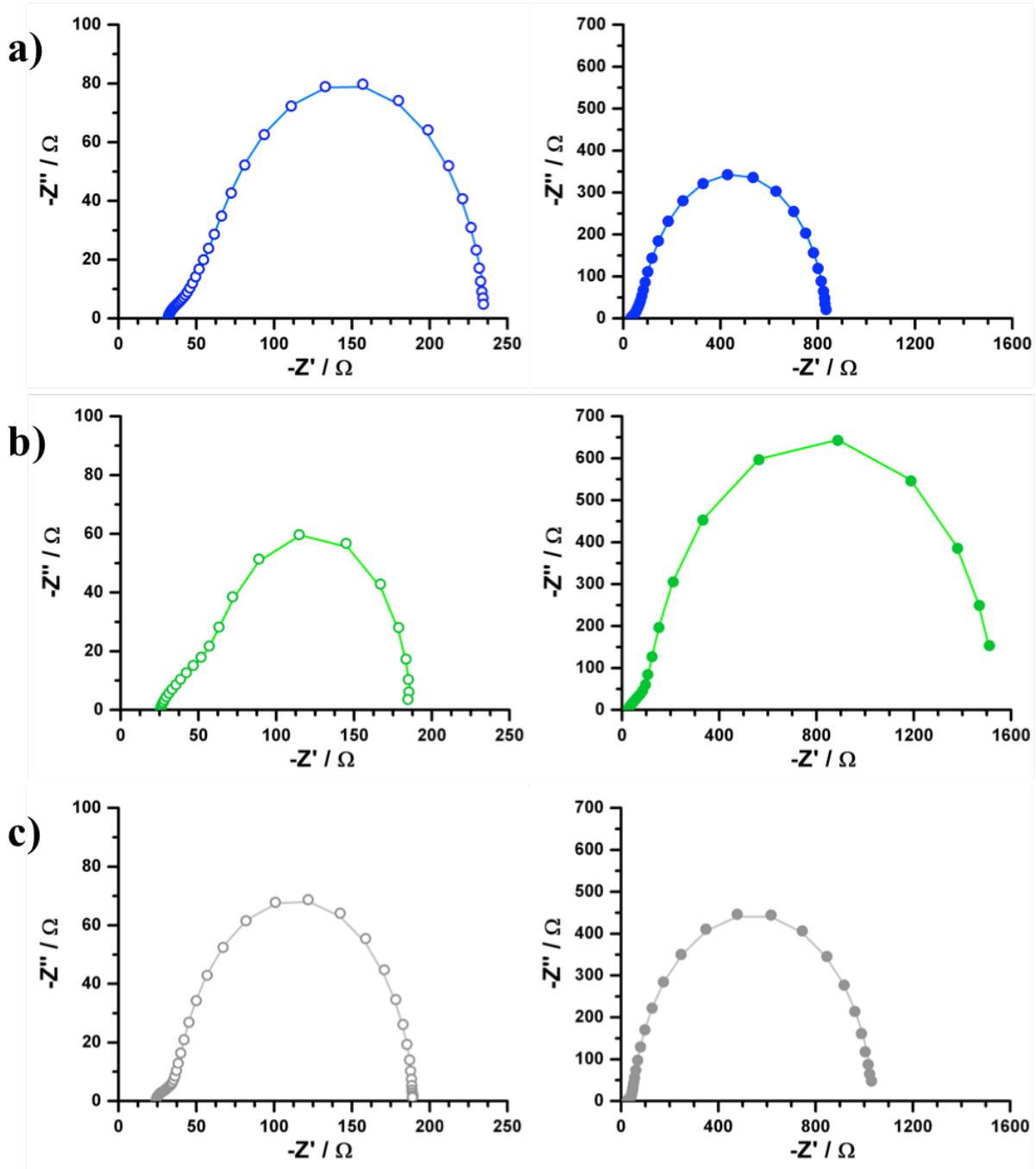


**Figure S14** Nyquist plots of EIS data determined for p-type NiO DSSCs sensitized with **P1** (a), **P2** (b), and **P3** (c) measured under light (open circles) and dark (filled circles) conditions. Fittings to the model in Figure S13 are presented by lines.

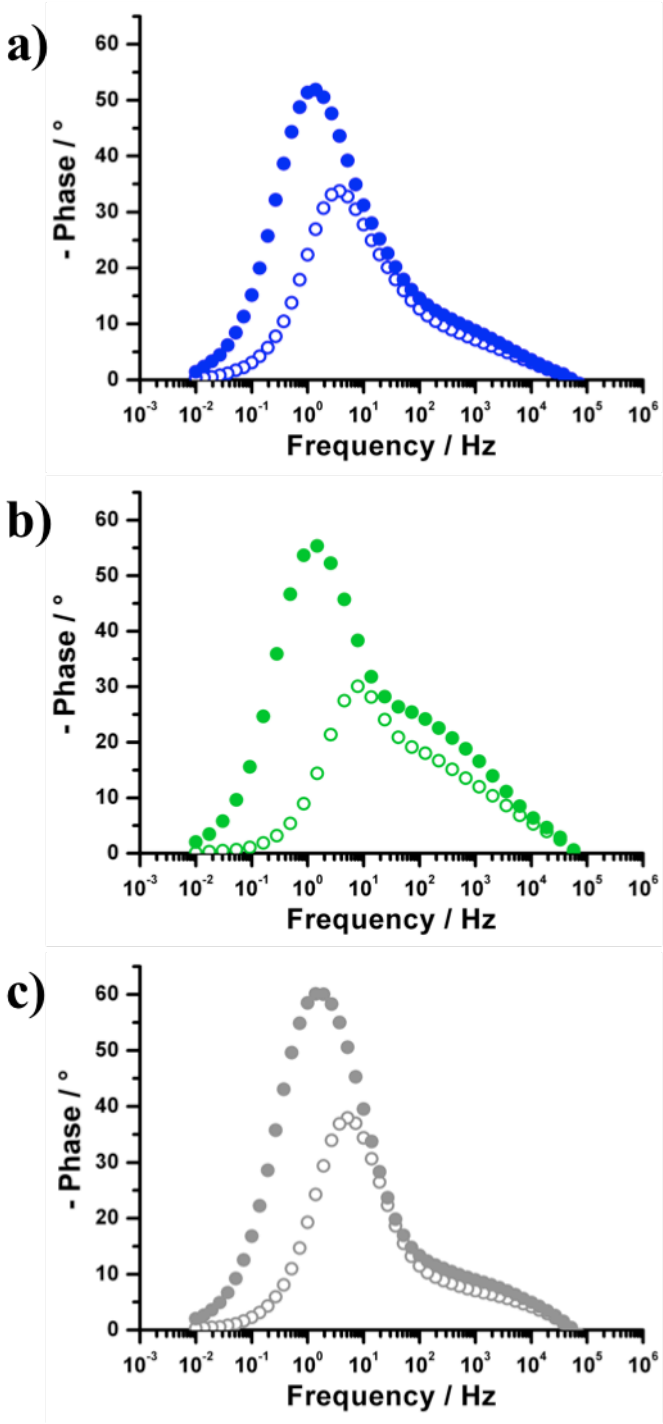


**Figure S15** Bode phase plots of EIS data determined for p-type NiO DSSCs with **P1** (a), **P2** (b), and **P3** (c) measured under light (open circles) and dark (filled circles) conditions.

**Table S1** Extinction coefficients (ε) and positions of Soret- and Q-bands of **P1** – **P3** in DMF, c = $10^{-5}$ M.

| | **P1** | | **P2** | | **P3** | | Free Base[a, 15] | |
|---|---|---|---|---|---|---|---|---|
| | ε / $M^{-1}\cdot cm^{-1}$ | λ(ε) / nm | ε / $M^{-1}\cdot cm^{-1}$ | λ(ε) / nm | ε / $M^{-1}\cdot cm^{-1}$ | λ(ε) / nm | ε / $M^{-1}\cdot cm^{-1}$ | λ(ε) / nm |
| Soret-band | 45900 | 395 | 34200 | 407 | 58300 | 412 | 115000 | 375 |
| Q-band | 25100 | 620 | 23000 | 628 | 40300 | 628 | 40000 (640 nm) | 570, 602, 640 |

[a] Spectrum of Free Base porphycene was recorded in THF. [15]

**Table S2** Reduction and oxidation potentials calculated versus normal hydrogen electrode (NHE) of porphycenes **P1** – **P3**. Reduction and oxidation potentials of porphyrins, which are comparable in the structure of the core, are added for comparison. [16-18]

| Porphycenes | Red. vs. NHE / V | Ox. vs. NHE / V |
|---|---|---|
| **P1** | - 0.80 | 0.98 |
| **P2** | - 0.88 | 1.02 |
| **P3** | - 0.99 | 0.89 |
| Porphyrins | Red. vs. NHE / V | Ox. vs. NHE / V |
| **(TPP)Ni**[a] | - 1.24 | 0.89 |
| **(TPrP)Ni**[b] | -1.10 | 0.75 |

[a] Measurements were carried out in dimethylformamid (DMF) containing 0.1 M of tetrabutylammonium perchlorat (TBAP) as supporting electrolyte and ferrocene/ferrocenium ($Fc/Fc^+$) redox couple as reference, (5,10,15,20-tetraphenylporphyrinato)$Ni^{II}$.

[b] Measurements were carried out in dimethylformamid (DMF) containing 0.1 M of tetrabutylammonium perchlorat (TBAP) as supporting electrolyte, (TPrP)Ni = (5,10,15,20-tetrapropylporphyrinato)$Ni^{II}$. A saturated calomel electrode was used as a reference ( $E_{redox}$ = 0.2444 vs. NHE). [19]

**Table S3** Summary of device performances of p-type NiO based DSSCs incorporating **P1** – **P3** as sensitizers.

| | $V_{oc}$ / V[a] | $J_{sc}$ / mA·cm$^{-2}$[b] | FF[c] | η / %[d] |
|---|---|---|---|---|
| **P1** | 0.071 | 0.767 | 0.37 | 0.019 |
| **P2** | 0.078 | 1.034 | 0.35 | 0.028 |
| **P3** | 0.068 | 0.823 | 0.38 | 0.021 |

[a] $V_{oc}$ = open-circuit voltage. [b] $J_{sc}$ = short-circuit current density. [c] FF = fill factor. [d] η = efficiency.

**Table S4** Summed Coulson atomic charges on dye, bridge and NiO for the ground (GS) and excited states (ES) of **P1** and **P2**.

| | **P1 GS** | **P1 ES** | **P2 GS** | **P2 ES** |
|---|---|---|---|---|
| Dye | -0.149 | 0.138 | -0.006 | -0.034 |
| Bridge | -1.177 | -1.053 | -1.327 | -1.318 |
| NiO | 1.329 | 0.919 | 1.330 | 1.357 |

**Table S5** Summary of EIS results by fitting the Nyquist plots of the corresponding data obtained under illumination conditions (AM 1.5, 100 mWcm$^{-2}$).

| | $R_i$ / Ω[a] | $C_2$ / μF[b] | $\tau_h$ / ms[c] | $k_{eff}$ / s$^{-1}$[d] |
|---|---|---|---|---|
| **P1** | 161.7 ± 6.9 | 622.4 | 42.7 | 1.39 |
| **P2** | 113.07 ± 5.5 | 369.4 | 20.2 | 4.52 |
| **P3** | 150.0 7 ± 1.0 | 482.1 | 30.7 | 1.93 |

[a] $R_i$ = resistance at the interface NiO electrode/chromophore, [b] $C_2$ = pseudo capacitance calculated from the $CPE_2$, [c] $\tau_h$ = hole lifetime, [d] $k_{eff}$ = recombination at the interface NiO electrode/chromophore.

**Table S6** Summary of EIS results by fitting the Nyquist plots of the corresponding data obtained under dark conditions.

| | $R_d$ / Ω[a] | $C_2$ / μF[b] | $\tau_h$ / ms[c] |
|---|---|---|---|
| **P1** | 729.93 7 ± 10.4 | 640.5 | 114.5 |
| **P2** | 1421.5 7 ± 13.0 | 360.8 | 107.0 |
| **P3** | 988.93 7 ± 4.7 | 505.5 | 114.5 |

[a] $R_d$ = resistance at the interface NiO electrode/electrolyte under dark conditions, [b] $C_2$ = pseudo capacitance calculated from the $CPE_2$, [c] $\tau_h$ = hole lifetime in the dark.

References


1. E. Vogel, M. Balci, K. Pramod, P. Koch, J. Lex and O. Ermer, *Angew. Chem.*, 1987, **99**, 909.

2. E. Vogel, M. Balci, K. Pramod, P. Koch, J. Lex and O. Ermer, *Angew. Chem. Int.. Ed.*, 1987, **26**, 928.

3. W. M. Campbell, K. W. Jolley, P. Wagner, K. Wagner, P. J. Walsh, K. C. Gordon, L. Schmidt-Mende, M. K. Nazeeruddin, Q. Wang, M. Grätzel and D. L. Officer, *J. Phys. Chem. C*, 2007, **111**, 11760.

4. S. Sumikura, S. Mori, S. Shimizu, H. Usami and E. Suzuki, *J. Photochem. Photobiol. A*, 2008, **199**, 1.

5. Z. Huang, G. Natu, Z. Ji, P. Hasin and Y. Wu, *J. Phys. Chem. C*, 2011, **115**, 25109.

6. S. Feihl, R. D. Costa, S. Pflock, C. Schmidt, J. Schonamsgruber, S. Backes, A. Hirsch and D. M. Guldi, *RSC Adv.*, 2012, **2**, 11495.

7. M. Adachi, M. Sakamoto, J. Jiu, Y. Ogata and S. Isoda, *J. Phys. Chem. B*, 2006, **110**, 13872.

8. R. Kern, R. Sastrawan, J. Ferber, R. Stangl and J. Luther, *Electrochimica Acta*, 2002, **47**, 4213.

9. Z. Huang, G. Natu, Z. Ji, M. He, M. Yu and Y. Wu, *J. Phys. Chem. C*, 2012, **116**, 26239.

10. Q. Wang, J.-E. Moser and M. Grätzel, *J. Phys. Chem. B*, 2005, **109**, 14945.

11. P. O. Dral and T. Clark, *J. Phys. Chem. A*, 2011, **115**, 11303.

12. A. A. T. Clark, B. Beck, F. Burkhardt, J. Chandrasekhar, P. Gedeck, A. Horn, M. Hutter, B. Martin, P. O. Dral, G. Rauhut, W. Sauer, T. Schindler, and T. Steinke, *VAMP 11.0*, Erlangen, 2011.

13. J. P. Stewart, *J Mol Model*, 2007, **13**, 1173.

14. T. Clark and J. Chandrasekhar, *Isr. J. Chem.*, 1993, **33**, 435.

15. N. Jux, C. Oelsner, D. M. Guldi, J. Malig and W. Brenner, *J. Porphyrins Phthalocyanines*, 2012, **16**, 651.

16. K. M. Kadish, M. M. Franzen, B. C. Han, C. Araullo-McAdams and D. Sazou, *Inorg. Chem.*, 1992, **31**, 4399.

17. A. M. Stolzenberg and M. T. Stershic, *J. Am. Chem. Soc.*, 1988, **110**, 6391.

18. D. Chang, T. Malinski, A. Ulman and K. M. Kadish, *Inorg. Chem.*, 1984, **23**, 817.

19. R. D. Caton, *J. Chem. Educ.*, 1973, **50**, A571.